Reduced graphene oxide/α-Fe₂O₃ fibres as active material for supercapacitor application

Gabrijela Radić[1], Ivan Šajnović[1], Željka Petrović[2,*], Marijana Kraljić Roković[1,*]

[1]*University of Zagreb, Faculty of Chemical Engineering and Technology, Department of Electrochemistry, Marulićev trg 19, 10000 Zagreb, Croatia*
[2]*Ruđer Bošković Institute, Division of Materials Chemistry, Bijenička cesta 54, P.O. Box 180, HR-10002, Zagreb, Croatia*

*Corresponding author's e-mail addresses: zpetrov@irb.hr; mkralj@fkit.hr

Keywords: composite, hematite fibres, hydrothermal method, reduced graphene oxide, supercapacitor

Abstract

The composite hydrogel, composed of reduced graphene oxide and α-Fe$_2$O$_3$ fibres (rGO/α-Fe$_2$O$_3$), was successfully prepared by the hydrothermal procedure starting from GO and α-Fe$_2$O$_3$ nanofibers. According to the SEM and XRD results, α-Fe$_2$O$_3$ fibres are distributed between rGO sheets increasing the inter-sheet space. The rGO/α-Fe$_2$O$_3$ composite was tested as an active material in supercapacitor by means of cyclic voltammetry, galvanostatic charging/discharging and electrochemical impedance spectroscopy in 0.5 mol dm^{-3} Na$_2$SO$_4$. The obtained results confirmed a positive effect of the α-Fe$_2$O$_3$ addition on capacitive properties. Improved capacitive properties of the composite make this material suitable for supercapacitor application.

Sazetak

Kompozitni hidrogel rGO/α-Fe$_2$O$_3$ pripremljen je hidrotermičkom metodom iz otopine grafenova oksida i nanovlakana hematita. Prema SEM i XRD rezultatima utvrđeno je da su vlakna hematita raspoređena između slojeva rGO čime je povećan njihov razmak. Kompozit rGO/α-Fe$_2$O$_3$ je ispitan kao potencijalni materijal za superkondenzatore primjenom cikličke voltametrije, galvanostatskih testova punjenja/pražnjenja i elektrokemijske impedancijske spektroskopije u 0.5 mol dm^{-3} Na$_2$SO$_4$. Dobiveni rezultati su potvrdili pozitivan utjecaj dodatka vlakana na kapacitivna svojstva kompozita. Poboljšana kapacitivna svojstva kompozita čine ovaj materijal pogodnim za primjenu u superkondenzatorima.

Introduction

The increasing demands for new energy sources have motivated researchers to improve energy conversion and to design and develop energy storage devices like lithium ion batteries and supercapacitors.[1-3] Since 1990s lithium-ion batteries have found applications in many portable electronic devices due to high energy density and good safety.[1,4] In contrast, supercapacitors are an attractive alternative to batteries because they can provide higher power density, electrochemical stability, long cycle life and fast charge-discharge process but suffer from lower energy density.[1,5,6] For successful application of supercapacitors in hybrid electric vehicles and energy management, both high power and energy densities are required.[1,5] Therefore, much effort has been made to achieve these demands.

One approach includes a development of low-cost, environmentally friendly and high-performance electrode material systems based on the design of different material combinations, morphology and particle size.[1,4,5-8] A promising strategy would be a combination of a capacitive material with an earth-abundant, nontoxic and low-cost metal oxide.[5,9] Resulting composite would have enhanced electrochemical properties important for its application in supercapacitors. According to the literature, synergistic effect of graphene and semiconductors like TiO_2, ZnO, SnO_2, Co_3O_4, MnO_2, CdS, $CdSe$, $BiVO_4$, Fe_2O_3, and Fe_3O_4 has been investigated.[1-3,7,10-14] These oxides lack electrical conductivity, but their combination with carbon materials (carbon black, carbon nanotubes, or graphene), which have superior capacitance characteristics, provides good electrical conductivity and mechanical stability during charge-discharge cycling.[7]

Among carbon materials, graphene has a large surface area, high electrical conductivity, good flexibility, wide potential window and high charge storage ability. Additionally, its two-dimensional structure makes it very suitable for fabrication of composites with other electrochemically active materials like metal oxides and conducting polymers.[1,15] Graphene obtained by a wet chemical method is known as reduced graphene oxide (rGO). rGO contains a certain amount of oxygen functional groups that are not completely removed during the reduction process and it also contains the defects that decrease electron conductivity characteristic for the perfect graphene lattice. Besides that, this modified structure shows additional features, which may be useful for its practical application. In the previous reports it was shown that energy storage properties can be improved by a pseudocapacitive effect of oxygen functional groups.[16-20] It was also reported that oxygen functional groups can be used for chemical attachment of *o*-phenylenediamine in order to improve pseudocapacitive properties.[20]

One of the most stable iron oxides under ambient conditions is hematite (α-Fe_2O_3), which possesses nontoxicity, is earth-abundant and has a low-cost of production. Due to many advantages like variable oxidation states it is used in both traditional and advanced technologies such as pigments, gas sensors, and photo-catalysts.[2,3,11,12,21,22] However, the low electrical conductivity (10^{-14} S cm^{-1}), low optical absorption coefficient, volume expansion during charge/discharge cycles, and capacity retention limit its practical use.[2,3,23]

Therefore, in this work the strategy for the preparation of a composite material with improved electrochemical properties has been applied. α-Fe_2O_3 nanofibers were incorporated within rGO (rGO/α-Fe_2O_3) in order to investigate synergistic effects between them and potential use as an efficient active material for supercapacitors. According to the literature data various

methodologies have been applied to produce graphene/metal oxide composites, like electrospinning,[24] hydrothermal/solvothermal method,[11] or cold spray coating process.[7] Among mentioned methods, the *in situ* wet chemical way using graphene oxide (GO) and metal salt as reactants during the synthesis, is the most commonly used.[25] In this work α-Fe_2O_3 nanofibers were first synthesised by the electrospinning method. In the second step, a composite material rGO/α-Fe_2O_3 was prepared hydrothermally from a solution containing GO and α-Fe_2O_3 nanofibers. Capacitive properties of the prepared composite were explored by cyclic voltammetry, chronopotentiometry and electrochemical impedance spectroscopy. As mentioned before, although the chosen material combination is known from previous investigations, we believe that this is the first work in which the composite preparation includes hydrothermal synthesis of rGO in the presence of oxide nanofibers.

Experimental section

Chemicals and solutions

Polyvinylpyrrolidone (PVP, M.W. = 1,300,000; *Alfa Aesar*®), Absolute ethanol (C_2H_5OH, p.a.; *Gram-mol*®), Acetic acid glacial ($C_2H_4O_2$, 99.9+%; *Alfa Aesar*®), Iron(III) nitrate nonahydrate ($Fe(NO_3)_3 \cdot 9H_2O$, p.a.; *Kemika*®), Sodium sulfate anhydrous (Na_2SO_4, p.a., *Kemika*®) were used as received. Aqueous solutions of 0.5 mol dm^{-3} Na_2SO_4 and 2.0 mol dm^{-3} $Fe(NO_3)_3 \cdot 9H_2O$ were prepared with deionised water. A PVP solution was prepared by mixing 3.0 g PVP, 50 ml C_2H_5OH and 5 ml deionised H_2O at 350 rpm, 70 ^{o}C during 6h.

Synthesis of electrospun fibres of iron oxide

Electrospun fibres were synthesized according to the published procedure.[26] The concentration of $Fe(NO_3)_3 \cdot 9H_2O$ solution for preparing electrospun fibres was 0.1 mol dm^{-3}. It was prepared by the addition of 2 mol dm^{-3} $Fe(NO_3)_3 \cdot 9H_2O$ to viscous PVP solution (pH was adjusted to 1 by acetic acid glacial) and stirred at 350 rpm and 70 ^{o}C for 1h. The electrospinning system was manufactured by *Linari Engineering*® s.r.l.u. and consisted of 40 kV high voltage generator, control panel, syringe pump and fibre collector covered by Al foil. The distance between the metallic nozzle tip (φ = 1.0 mm) and the Al collector was 10 cm, the flow of viscous solution was 1 cm^3 h^{-1}, and the high voltage was 10 kV. The electrospun fibres were thermally treated in a preheated furnace at 700 °C during 1 hour in order to remove an organic part of the fibres and form an iron oxide. The fibres, thus prepared, were used to synthesis a composite material.

Synthesis of graphene oxide (GO)

GO was synthesized from graphite powder according to the Hummers´ procedure.[27] In a typical procedure, 3.0 g of graphite and 1.5 g NaNO$_3$ was mixed with 69 mL of concentrated sulphuric acid under a constant stirring in an ice bath where the temperature close to 0°C was reached. Afterwards, 9.0 g of potassium permanganate was added gradually to the solution while the temperature was kept below 20°C. After 20 minutes, the flask was moved to a water bath and the solution was stirred at 35°C for 30 min. The resulting solution was diluted by gradually adding 120 cm^3 of water and maintaining the temperature at 98 °C for 0.5 h. Next, the flask was cooled to room temperature after which the mixture was poured into 420 cm^3 of water with vigorous stirring, and 30% H$_2$O$_2$ was added to the solution in order to quench the reaction and remove the excess oxidant. The resulting mixture was washed with 5% HCl and deionised water by using centrifugation until the pH value approached 7.0. Graphene oxide suspension was prepared by the ultrasonication of graphite oxide in deionised water (40 kHz) during one hour and centrifuged at 4000 rpm to remove any non-exfoliated graphite oxide particles. The GO concentration was 6.7 mg cm^{-3}.

Synthesis of composite material – (rGO/iron oxide fibres)

Synthesis of a composite material was carried out hydrothermally using iron oxide fibres and GO suspension. Two types of samples were synthesized: (i) reference sample – rGO hydrogel (denoted as rGO1) and (ii) composite sample containing rGO and 1w% of fibres – rGO/α-Fe$_2$O$_3$ hydrogel (denoted as rGO2).

For a synthesis of rGO1 sample, 5.97 cm^3 of GO suspension (6.7 mg cm^{-3}) and 10 cm^3 of olive leaf extract solution (2.8w%) were mixed and an appropriate amount of deionised H$_2$O was added to form a 20 cm^3 reaction mixture in order to obtain a GO concentration of 2 mg cm^{-3}. The olive leaf extract served as a reducing agent.[28] In the case of rGO2 sample the same procedure was used as for rGO1 except an appropriate amount of fibres was added to the reaction mixture and ultrasonically dispersed during 10 minutes. pH value was 4 in both cases. Finally, the prepared reaction mixtures were put in autoclaves at 50 °C during 1 hour and then gradually heated up to 120 °C and left for 5 hours. Afterward, the autoclaves were gradually cooled to room temperature and the samples, in the form of hydrogels, were washed with deionized water several times and freeze-dried in order to obtain an aerogel. After the synthesis, morphological and electrochemical characterisations of the samples were carried out.

Characterization of samples

The morphology of prepared samples was inspected with a *Jeol Ltd.* thermal field emission scanning electron microscope (FE-SEM, model JSM-7000F). The FE-SEM was coupled with *Oxford Instruments* EDS/ INCA 350 (energy dispersive X-ray analyser). XRD diffractometer (model APD 2000) manufactured by *Italstructures* was used to identify the phase composition. The XRD patterns were recorded with Cu$K\alpha$ radiation at 40 kV and 30 mA in the 2θ range from 8 to 70°.

All electrochemical experiments were carried out in an aqueous solution of Na_2SO_4 at room temperature in a two-electrode cell and for this purpose two symmetric supercapacitors were prepared. The supercapacitor SC1 was assembled using a nickel sheet (1 cm^2) and by applying a piece of active material rGO1 hydrogel on the nickel surface. The supercapacitor SC2 was assembled in the same way except that rGO2 hydrogel was used. The hydrogel was obtained by soaking the aerogel in Na_2SO_4 solution during the night. The electrodes were separated by glass paper fibres wetted with 0.5 mol dm^{-3} Na_2SO_4 solutions. The supercapacitor was then placed in an outer casing, in order to prevent electrolyte evaporation, and pressed between two glass plates using clamps.

The galvanostatic charge-discharge (GCD) measurements were performed at a current value of 0.80 or 1.46 A g^{-1} in the voltage range between 0 and 1.2 V. The cyclic voltammetry (CV) measurements were carried out at a scan rate of 50 mV s^{-1} in the voltage range between 0 and 1.2 V. The impedance measurements (EIS) were performed in the frequency range between 10^5 and 10^{-3} Hz using an *ac* voltage amplitude of ±5 mV at a *dc* voltage of 0 V. All measurements were conducted using a potentiostat/galvanostat (*EG&G Princeton Applied Research*, model 263A) with a frequency response analyser (*EG&G Princeton Applied Research*, model 5210). The impedance spectra were analysed using the software *ZView*® for complex-linear least squares (CNLS) developed by Boukamp.[29]

Results and Discussion

Morphological and structural characteristics of electrospun fibres

The morphology of electrospun fibres, which were used for the preparation of a composite material, was examined by SEM and shown in Fig. 1a. As can be seen from Fig. 1a a single fibre is composed of interconnected nanoparticles, which represent an inorganic phase, since an organic part of fibres was decomposed during the thermal treatment (700 °C, 1 hour). An average value of a fibre diameter amounts to 61±14 nm.

The chemical and phase composition of nanofibers was investigated by EDS and XRD techniques. The EDS spectrum (Fig.1b) of the selected area (Fig 1a) is shown together with the results of element analysis. The nanofibers consisted of 63.95 atomic% of oxygen and 36.05 atomic% of iron which is close to the stoichiometric ratio characteristic for hematite, α-Fe_2O_3, O:Fe = 60:40.

The confirmation of the hematite phase is also observed from the diffraction pattern of the nanofibers (Fig 1c). Experimental data were compared with a reference pattern for hematite, JCPDS-ICDD PDF card No. 33-0664.[30] According to the diffractogram, the fibres have showed only the presence of lines characteristic for the hematite, α-Fe_2O_3. No other phase was detected in the sample. The hematite nanofibers were used for the preparation of the rGO/α-Fe_2O_3 composite.

Morphological and structural characteristics of rGO1 and rGO2 samples
The morphology of the reference, rGO1 and composite, rGO2 sample was investigated by SEM and the obtained micrographs are shown in Fig. 2. The rGO1 aerogel is composed of many wrinkled sheets that create a porous structure (Fig. 2a). In Figs. 2b and c the surface of the composite sample rGO2 is visible. As can be noticed, α-Fe_2O_3 fibres are distributed on the surface (Fig. 2b) and between rGO sheets (Fig. 2c). Such distribution of fibres increases the inter-sheet space and decreases the stacking of rGO sheets.[31-33] Additionally, a fibril structure was preserved during the hydrothermal treatment. If α-Fe_2O_3 fibres from Fig. 1a are compared with fibres in the composite, it is clearly visible that the average diameter of fibres in rGO2 sample is much larger and amounts around 700 nm. Evidently, a fusion of the fibres occurred during the synthesis of the composite (120 °C for 5 hours). According to the EDS results, graphene sheets in the rGO2 sample are consisted of 75 atomic% of carbon and 25 atomic% of oxygen which is very close to rGO1 (reference) sample, in which the ratio C:O = 70:30 atomic%. The important conclusions arise from the obtained results: (i) similar reduction efficiency of GO into rGO was obtained without and in the presence of α-Fe_2O_3 fibres and (ii) the fibres are wrapped with the rGO layers. The results are comparable with morphological characteristics of the rGO/hematite in the works of D.M.G.T. Nathan,[2] C.M. Subramaniyam,[4] and J.G. Lee.[7]

In order to determine the influence of α-Fe_2O_3 on structural properties of the rGO2, the prepared samples were analysed with XRD, Figure 3. The obtained results show for rGO1 a broad diffraction peak centred at 24° (corresponding to a *d*-spacing value or interlayer

distance of 3.71Å). This peak was assigned to the c (002) reflection of the graphite derived from the short-range order in stacked graphene sheets indicating a significant reduction of GO after the hydrothermal process.[34,35] Similar diffraction peak was registered in the case of rGO2 what means that stacking also occurred in the case of rGO2. However, the diffraction peak obtained for rGO2 moves to 23°, which corresponds to higher *d*-spacing value, *d* = 3.88 Å. Therefore it was concluded that although stacking was not prevented completely, the presence of α-Fe_2O_3 influenced structural properties of rGO2. Additional diffraction peaks, visible in diffractogram of the rGO2, are characteristic for the hematite phase α-Fe_2O_3 (JCPDS no. 33-0664) and for impurities present within the sample. The most probably impurities can be correlated to Na_2SO_4 (JCPDS 96-101-0523) in which rGO2 sample was stored. Despite intensive washing, Na_2SO_4 was not completely removed.

Electrochemical performances of rGO1 and rGO2

The electrochemical charge storage characteristics of prepared samples were investigated by assembling supercapacitors SC1 and SC2 with rGO1 and rGO2 active materials, respectively. Three different techniques, cyclic voltammetry (CV), galvanostatic charge/discharge (GCD), and electrochemical impedance spectroscopy (EIS) measurements were used. All measurements were done in a two-electrode system.

Fig. 4 presents the CV curves of the SC1 supercapacitor (a, b) and the SC2 supercapacitor (c, d) recorded at a scan rate of 50 mV s^{-1} before (a, c) and after (b, d) charge/discharge tests. It is well known that an ideal capacitor should retain a constant current during CV scans according to the relation $I(t) = C (dU/dt)$, where *I* is the current, *U* is the voltage and *t* is the time.[36-38]] Although CV curves of both supercapacitors are characterized by a good capacitive, almost rectangular CV shape, SC2 shows higher specific currents (Fig. 4cd) and a smaller deviation from the rectangular shape compared to SC1 (Fig. 4ab). The polarisation of each electrode was carried out by changing the polarity that resulted in two cyclic voltamograms, one from 0 V to 1.2 V and the other from 0 V to -1.2 V. The same response was obtained by applying a positive or a negative charge at each electrode, as it is evident from CV responses. This behaviour is quite reasonable since the symmetric supercapacitors were tested. However, after 1000 cycles of GCD (Fig. 5), a different behaviour was observed. CV responses at positive voltage values, i.e. responses obtained by using the same electrode polarity that was used for GCD tests (from 0 to 1.2 V), are significantly different before (Fig. 4a, c) and after GCD test (Fig. 4b, d). CV responses at negative voltage values, i.e. responses obtained by using the opposite polarity than those used for GCD tests (from 0 to -1.2 V), are almost the same before

and after GCD. From the obtained results it can be concluded that the degradation of active material during GCD test was different for each electrode. Similar effect was obtained for supercapacitor SC1 and supercapacitor SC2 indicating that the presence of α-Fe$_2$O$_3$ did not significantly influence the stability of the active material.

The specific capacitance (C_s/Fg^{-1}) values of the prepared electrodes were calculated using equation (1) and the results are shown in Table 1.

$$C_S = \frac{\int_{0\,V}^{1.2V} I dE}{2\Delta U m} \tag{1}$$

In equation (1), Q/C is the sum of anodic and cathodic charges obtained by the integration of the cyclic voltammograms in the voltage range ΔU/V, and m/g is the mass of the active material at one electrode.

From Table 1 it is evident that C_s in the negative voltage range has not been changed while C_s values in the positive voltage range were different before and after 1000 cycles of charging/discharging, which supports the previous conclusion. It is also evident that higher C_s values are registered for SC2 compared to SC1. It can be explained by the influence of α-Fe$_2$O$_3$ fibres on structural properties of the composite material. As it was shown before, α-Fe$_2$O$_3$ fibres are incorporated between rGO layers (see Fig. 2bc) decreasing an agglomeration of rGO and increasing its surface area available for a charge/discharge process. Consequently, specific capacitance values are increased. The response characteristic for pseudocapacitive redox reaction of α-Fe$_2$O$_3$ was not noticed in our experiment and therefore we believe that a pseudocapacitive redox reaction of α-Fe$_2$O$_3$ does not take place.

The long-term stability of the prepared samples was investigated by the GCD test during 1000 cycles and the results are shown in Fig. 5. GCD profiles were recorded at selected current densities in the voltage range from 0 to 1.2 V. Both GCD profiles exhibit three different regions for charging and three different regions for discharging processes:[36] (i) stabilization period in the first 5 s at the open circuit potential (OCP), (ii) *IR* drop caused by the internal system resistance, (iii) charging/discharging profile. During the discharging process, a linear relationship between voltage and time is obtained, while the relationship obtained during the charging process is not linear and this deviation is more pronounced for the SC1 supercapacitor. The linear relationship between voltage and time indicates a double layer characteristic and good capacitive behaviour of the investigated system. The difference between these two capacitors can be explained by the influence of α-Fe$_2$O$_3$ fibres on rGO

capacitive properties. The linear GCD response is in accordance with the CV results (Fig. 4) and it also indicates better capacitive behaviour of the SC2 supercapacitor.

From the galvanostatic discharge curves gravimetric specific capacitances (C_s) of investigated samples were calculated according to the equation (2):[23, 36]

$$C_s = \frac{I \cdot \Delta t}{m \cdot \Delta U} \tag{2}$$

where C_s is the specific capacitance of the cell, I is the constant current, Δt is the discharging time, m is the total weight of one electrode active material, and ΔU is the voltage drop during the discharging process. The obtained C_s values are shown in Table 2. As can be seen the obtained capacitance values of the SC2 supercapacitor are higher compared to the values of the SC1 supercapacitor confirming better capacitive behaviour of SC2. The results are in a good agreement with the CV results.

Specific energy (E_s), and specific power (P_s), as key parameters for fabricating energy storage devices, were calculated according to the equations:[36, 39]

$$E_s = 0.5 \cdot C_s \cdot \Delta U^2 \tag{3}$$

$$P_s = \Delta U^2 / (4m \cdot ESR) \tag{4}$$

where ESR is the electrical series resistance, which represents total internal resistance of a capacitor that includes electrolyte, contact, active material and separator resistances.[5,39, 40] ESR was calculated from the voltage drop of the galvanostatic discharge curve (IR drop). ESR values for the SC1 ranged from 34 Ω to 42 Ω, while for the SC2 values ranged from 35 Ω to 40 Ω. According to the obtained values it can be concluded that there is no significant difference between these two supercapacitors. All calculated parameters are listed in Table 2. The calculated specific energy values are similar for both supercapacitors, although higher C_s values were registered for the SC2. However, a more significant voltage drop due to the open circuit discharge in the case of SC2 (see Fig. 5b) has affected the reduction in the amount of stored specific energy and specific power of the supercapacitor. The energy and power values calculated in this work are in accordance with the literature[41-43] and they indicate high power capability of the prepared supercapacitors.

Electrochemical impedance spectroscopy (EIS) was used for *in situ* study of current collector/active material and active material/electrolyte interfaces of investigated supercapacitors. Impedance spectra of the SC1 and SC2 supercapacitors, recorded in 0.5 mol dm^{-3} Na$_2$SO$_4$, are presented in the form of Nyquist and Bode plots in Fig. 6. As can be seen from Fig. 6, the appearance of parasitic inductive impedance (positive imaginary part of

impedance) can be noticed at the highest frequencies. At higher frequencies, a capacitive loop for both samples is observed. This capacitive loop can be described by the charge transfer at the current collector or the formation of the interfacial region between the current collector and active material.[39,40,44] At high-to-medium frequencies a diffusional response due to the effect of electrode porosity (θ = -45°) followed by a capacitive response at lower frequencies is visible. Similar impedance responses were obtained for the supercapacitors based on carbon nanofibers/carbon nanosheets,[45] FeOx/rGO[46] and Fe_2O_3/rGO[12] systems.

The investigated systems are well described by the electrical equivalent circuit (EEC), shown as an inset in Fig. 6, which consists of the following elements: inductor (L) in series with electrolyte resistance (R_{HF}) followed by ($Q_1R_1W_o$) and constant phase element (Q_2). R_1 is the contact resistance and Q_1 is the double layer charging at the current collector/active material interface. W_o is the finite-length Warburg element for diffusion of electrolyte ions into the pores of the active material (rGO1 or rGO2). Q_2 represents the double layer charging at the active material/electrolyte interface. Because the measured capacitive response is not generally ideal due to certain heterogeneity of the electrode surface,[47] a constant phase element (CPE) has been introduced for fitting the spectra, instead of an ideal capacitance element. Its impedance can be defined by $Z(CPE) = [Q(j\omega)^n]^1$, where Q is a constant, ω is the angular frequency, and n is the CPE power. The factor n is an adjustable parameter, which has values between -1 and 1; a value of -1 is characteristic for an inductance, a value of 1 corresponds to a capacitor, a value of 0 corresponds to a resistor.[48] The values of impedance parameters, obtained by the performed analysis, are listed in Table 3. As evidenced from Table 3 and Fig. 6, a very good agreement between the experimental (symbols) and modelled data (solid lines) was obtained using the EEC presented as the inset in Fig. 6.

According to the results after charging/discharging of the SC1 and SC2 supercapacitors the most significant change was obtained for Q_1, R_1 and W_o elements. Since these elements represent the current collector/active material interface, changes at the current collector (Ni) surface and/or in the structure of active materials during these GCD tests can be assumed. The sums of $R_{HF}+R_1$ values, which represent *ESR*, are relatively close to the values obtained from the galvanostatic discharge *IR* drop (previous section of the text). A significant increase of Warburg resistance values (W_o-R) after GCD tests can be noticed for both samples, although it is more expressed in the SC1 values. This behaviour is, obviously, a consequence of pore diameter changes. According to SEM results (Fig. 2) an rGO structure is highly porous and it is well known that rGO sheets tend to restack. Since W_o-R values are increased, a restructuring of active material is possible during the polarization. Restructuring of active

material will change the pore size and as the pore diameter is reduced, the ion transport is more difficult. This phenomenon is significantly pronounced in the case of the SC1 supercapacitor whose W_o-R value is about 6 times higher after GCD test while for the SC2 supercapacitor it is only 1.5 times higher after GCD test. These results are in a good agreement with other electrochemical results and have confirmed a positive effect of the α-Fe_2O_3 fibres on the double layer capacitance properties of the rGO/α-Fe_2O_3 composite. The intercalation of hematite fibres in the rGO structure decreases rGO sheet restacking and minimizes structure changes. Therefore, the new composite material rGO/α-Fe_2O_3 possesses better capacitive properties in comparison to the bare rGO. These results have also showed that EIS method is more sensitive to changes in the supercapacitor structure in comparison to other electrochemical techniques. Therefore, it is a highly valuable technique for investigations of supercapacitor properties.

Conclusions

The composite hydrogel of rGO and α-Fe_2O_3 was successfully prepared by the hydrothermal procedure starting from GO and α-Fe_2O_3 nanofibers. According to SEM results a fibril structure of α-Fe_2O_3 was preserved during the hydrothermal treatment and intercalated within rGO sheets. The rGO restacking was decreased in the presence of α-Fe_2O_3 as proved by XRD.

Two different symmetric supercapacitors were prepared, one containing pure rGO and the other composite hydrogel. According to obtained results, an addition of α-Fe_2O_3 fibres to rGO had a positive effect on the electrochemical properties of the new composite material. Consequently specific capacitance values (C_s) of supercapacitor were increased from 17.5 F g^{-1} (bare rGO) to 26.2 F g^{-1}(composite rGO/α-Fe_2O_3). The results of EIS method indicated different structural properties of the used materials what is reflected in Warburg resistance values. The restructuring of the active material, that takes place during charging/discharging, is minimized by the presence of α-Fe_2O_3.

References

[1]   F. Zhang, T. Zhang, X. Yang, L. Zhang, K. Leng, Y. Huang, Y. Chen, *Energy Environ. Sci.* **2013**, *6*, 1623.

[2]   D. M. G. T. Natham, S. J. M. Boby, *J. Alloys Compd.* **2017**, *700*, 67.

[3]   S. A. Carminati, F. L. Souza, A. F. Nogueira, *ChemPhysChem* **2016**, *17*, 170.

[4]   C. M. Subramaniyam, Md. M. Islam, T. Akhter, D. Cardillo, K. Konstantinov, H. K. Liu, S. X. Dou, *RSC Adv.* **2016**, *6*, 82698.

[5]   G. Yu, L. M. Vosgueritchian, H. Wang, X. Xie, J. R. McDonough, X. Cui, Y. Cui, Z. Bao, *Nano Lett.* **2011**, *11*, 2905.

[6]   J. Eskusson, P. Rauwel, J. Nerut, A. Jänes, *J. Electrochem. Soc.* **2016**, *163*, A2768.

[7]   J.-G. Lee, B. N. Joshi, J.-H. Lee, T.-G. Kim, D.-Y. Kim, S. S. Al-Deyab, Il W. Seong, M. T. Swihart, W. Y. Yoon, S. S. Yoon, *Electrochim. Acta* **2017**, *228*, 604.

[8]   K. Wasinski, M. Walkowiak, P. Pòłrolniczak, G. Lota, *J. Power Sources* **2015**, *293*, 42.

[9]   S. Sopčić, N. Šešelj. M. Kraljić Roković, *J. Solid State Electrochem.* **2018**, doi: 10.1007/s10008-018-4122-9.

[10]   C. C. Hu, K. H. Chang, M. C. Lin, Y. T. Wu, *Nano Lett.* **2006**, *6*, 2690.

[11]   F. Meng, J. Li, S. K. Cushing, J. Bright, M. Zhi, J. D. Rowley, Z. Hong, A. Manivannan, A. D. Bristow, N. Wu, *ACS Catal.* **2013**, *3*, 746.

[12]   L. Liu, D. Wu, X. Shao, J. Wang, J. Nie, J. Sun, S. Wang, *Compos. Interfaces* **2017**, *24*, 257.

[13]   D. Sačer, M. Kralj, S. Sopčić, M. Košević, A. Dekanski, M. Kraljić Roković, *J. Serb. Chem. Soc.* **2017**, *82*, 411.

[14]   T. Cottineau, M. Toupin, T. Delahaye, T. Brousse, D. Bélanger, *Appl. Phys. A: Mater. Sci. Process* **2006**, *82*, 599.

[15]   D. Sačer, D. Čapeta, I. Šrut Rakić, R. Peter, M. Petravić, M. Kraljić Roković, *Electrochim. Acta* **2016**, *193*, 311.

[16]   H. Cao, X. Peng, M. Zhao, P. Liu, B. Xu, J. Guo, *RSC Adv.* **2018**, *8*, 2858.

[17]   B. Xu, S. Yue, Z. Sui, X. Zhang, S. Hou, G. Cao, Y. Yang, *Energy Environ. Sci.* **2011**, *4*, 2826.

[18]   S. H. Tamboli, B. S. Kim, G. Choi, H. Lee, D. Lee, U. M. Patil, J. Lim, S. B. Kulkarni, S. C. Jun, H. H. Cho, *J. Mater. Chem. A* **2014**, *2*, 5077.

[19]   Z. Liu, L. Jiang, L. Sheng, Q. Zhou, T. Wei, B. Zhang, Z. Fan, *Adv. Funct. Mater.* **2017**, *28*, 1705258.

[20]   D. Sačer, I. Spajić, M. Kraljić Roković, Z. Mandić, *J. Mater. Sci.* **2018**, *53*, 15285.

[21]   S. Krehula, G. Štefanić, K. Zadro, Lj. Kratofil, M. Marciuš, S. Musić, *J. Alloys Compd.* **2012**, *545*, 2009.

[22]   J. Štajdohar, M. Ristić, S. Musić, *J. Mol. Struct.* **2013**, *1044*, 290.

[23]   P. Liao, M. C. Toroker, E. A. Carter, *Nano Lett.* **2011**, *11*, 1775.

[24]   L. Guo, X. Kou, M. Ding, C. Wang, L. Dong, H. Zhang, C. Feng, Y. Sun, Y. Gao, P. Sun, G. Lu, *Sens. Actuators B* **2017**, *244*, 233.

[25]   D. Chen, H Quan, J. Liang, L. Guo, *Nanoscale* **2013**, *5*, 9684.

[26]   C. Eid, A. Brioude, V. Salles, J-C Plenet, R. Asmar, Y. Monteil, R. Khoury, A. Khoury, P. Miele, *Nanotechnology* **2010**, *21*, 125701.

[27]   D. C. Marcano, D V. Kosynkin, J. M. Berlin, A. Sinitskii, Z. Sun, A. Slesarev, L. B. Alemany, W. Lu, J. M. Tour, *ACS Nano* **2010**, *4*, 4806.

[28]   D. Sačer, F. Raffin, S. Sopčić, D. Antonić, M. Kraljić Roković, *Synthesis, Characterisation And Application Of Graphene Hydrogels*, 17th Ružička days, Vukovar, September, 19-21, 2018.

[29]   B.A. Boukamp, *Solid State Ionics* **1986**, *18-19*, 136.

[30]   Joint Committee on Powder Diffraction Standards, *Anal. Chem.* **1970**, *42*, 81A.

[31]   S. Park, J. An, I. Jung, R. D. Piner, S. J. An, X. Li, A. Velamakanni, R. S. Ruoff, *Nano Lett.* **2009**, *9*, 1593.

[32]   D. Li, M. B. Müller, S. Gilje, R. B. Kaner, G. G. Wallace, *Nat. Nanotechnol.* **2008**, *3*, 101.

[33]   H. Qian, L. Jinlong, L. Tongxiang, W. Chen, *J. Electrochem. Soc.* **2017**, *164*, E173.

[34]   H. H. Huang, K. K. H. De Silva, G. R. A. Kumara, M. Yoshimura, *Science* **2018**, *8*, 6849.

[35]   M. Fathy, A. Gomaa, F. A. Taher, M. M. El-Fass, A. E.-H. B. Kashyout, *J. Mater. Sci.* **2016**, *51*, 5664.

[36]   Y. Zheng, W. Pann, D. Zhengn, C. Sun, *J. Electrochem. Soc.* **2016**, *163* D230.

[37]   H. Yang, S. Kannappan, A. S. Pandian, J.- H. Jang, Y. S. Lee, W. Lu, *Nanotechnology* **2017**, *28*, 445401.

[38]   B. E. Conway, *Electrochemical Supercapacitors: Scientific Fundamentals and Technological Applications,* Springer, New York, **1999**, p. 105.

[39]   S. Sopčić, D. Antonić, Z. Mandić, K. Kvastek, V. Horvat-Radošević, J. *Electrochem. Sci. Eng.* **2018**, *8* 183.

[40]   T. Brousse, D. Bélanger, *Electrochem. Solid-State Lett.* **2003**, *6*, A244.

[41]   D. Bélanger, T. Brousse, J. W. Long, *Electrochem. Soc. Interface* **2008**, *17*, 49.

[42]   J. W. Long, D. Bélanger, T. Brousse, W. Sugimoto, M. B. Sassin, O. Crosnier, *MRS Bull*. **2011**, *36*, 513.

[43]   Y. Xu, Z. Lin, X. Zhong, X. Huang, N. O. Weiss, Y. Huang, X. Duan, *Nat. Commun*. **2014**, *5*, 4554.

[44]   J. Kim, S. C. Byun, S. Chung, S. Kim, *Carbon Lett*. **2018**, *25*, 14.

[45]   Y. Jiang, J. Yan, X. Wu, D. Shan, Q. Zhou, L. Jiang, D. Yang, Z. Fan, *J. Power Sources* **2016**, *307,* 190.

[46]   P.-C. Gao, P. A. Russo, D. E. Conte, S. Baek, F. Moser, N. Pinna, T. Brousse, F. Favier, *ChemElectroChem* **2014**, *1*, 747.

[47]   Z. Lukacs, *J. Electroanal. Chem*. **1997**, *432*, 79.

[48]   Z. Grubač, Ž. Petrović, J. Katić, M. Metikoš-Huković, R. Babić, *J. Electroanal. Chem.* **2010**, *645*, 87.

Table 1. Specific capacitance values (C_s) obtained for the SC1 and SC2 supercapacitors from CV responses. Different voltage ranges present a reverse polarity of electrodes in the supercapacitor.

Sample		C_s / F g^{-1} 0 V to -1.2 V	C_s / F g^{-1} 0 V to 1.2 V
SC1	before GCD	16.9	17.5
	after GCD	17.8	15.0
SC2	before GCD	23.0	26.2
	after GCD	22.6	20.4

Table 2. Values of specific capacitance (C_s), specific energy (E_s), and specific power (P_s) obtained from GCD tests at a different number of cycles for the SC1 and SC2 supercapacitors.

Sample	No. cycle	C_s / F g^{-1}	E_s / W h kg^{-1}	P_s / kW kg^{-1}
	2nd	18.7	3.07	17.1
	10	19.1	3.15	17.0
SC1	100	17.2	2.80	16.9
	200	16.5	2.66	16.3
	500	15.0	2.43	15.4
	1000	14.2	2.30	14.2
	2nd	24.1	2.95	4.52
	10	24.2	3.09	4.65
SC2	100	22.8	2.93	4.97
	200	21.5	2.74	4.78
	500	20.2	2.52	4.44
	1000	19.5	2.33	3.93

Table 3. Numerical values of impedance parameters for the SC1 and SC2 supercapacitors before and after the GCD test.

Sample	$L \cdot 10^6$ / H	R_{HF} / Ω	$Q_1 \cdot 10^4$ / $\Omega^{-1}\,s^{n1}$	n1	R_1 / Ω	$W_o\text{-}R$ / Ω	$W_o\text{-}T$ / s	$Q_2 \cdot 10^3$ / $\Omega^{-1}\,s^{n2}$	n2	$\chi^2 \cdot 10^3$
SC1 before GCD	1.51	1.39	1.95	0.77	30.5	45.4	1.41	4.99	0.92	1.29
SC1 after GCD	1.47	1.63	3.14	0.70	41.9	273	15.9	5.18	0.97	2.38
SC2 before GCD	1.04	2.39	1.10	0.78	38.4	29.6	2.71	23.2	0.86	1.04
SC2 after GCD	1.19	2.43	1.59	0.72	42.2	41.9	4.30	23.8	0.87	0.57

Figure captions

Figure 1. a) SEM image of fibres thermally prepared at 700 °C during 1 hour; 50000x magnification, b) EDS spectrum, and c) XRD pattern of fibres. Assignation of diffraction lines was done according to the JCPDS-ICDD PDF card No. 33-0664 (hematite, α-Fe$_2$O$_3$).

Figure 2. SEM images of: a) reference sample-rGO1 at 50000x; b) composite sample-rGO2 at 10000x; c) rGO2 at 33000x magnification.

Figure 3. XRD patterns of rGO1 and rGO2 samples recorded at 20 °C. Assignation of diffraction lines was done according to the JCPDS-ICDD PDF cards No. 33-0664 (hematite) and No. 96-101-0523 (Na$_2$SO$_4$).

Figure 4. Cyclic voltammograms of the SC1 (a,b) and SC2 (c,d) recorded within the potential range from 0 to 1.2 V in 0.5 mol dm^{-3} Na$_2$SO$_4$ at 50 mV s^{-1} before (a,c) and after (b,d) charge-discharge tests.

Figure 5. Galvanostatic charge/discharge profiles recorded in 0.5 mol dm^{-3} Na$_2$SO$_4$ during 1000 cycles for the: a) SC1 at $I_s = 0.80$ A g^{-1} and b) SC2 at $I_s = 1.46$ A g^{-1}.

Figure 6. Impedance spectra of the SC1 and SC2 supercapacitors recorded at 0 V in 0.5 mol dm^{-3} Na$_2$SO$_4$ before and after charge-discharge tests. Symbols represent experimental data and lines represent modelled data. The inset: EEC used to fit the spectra.
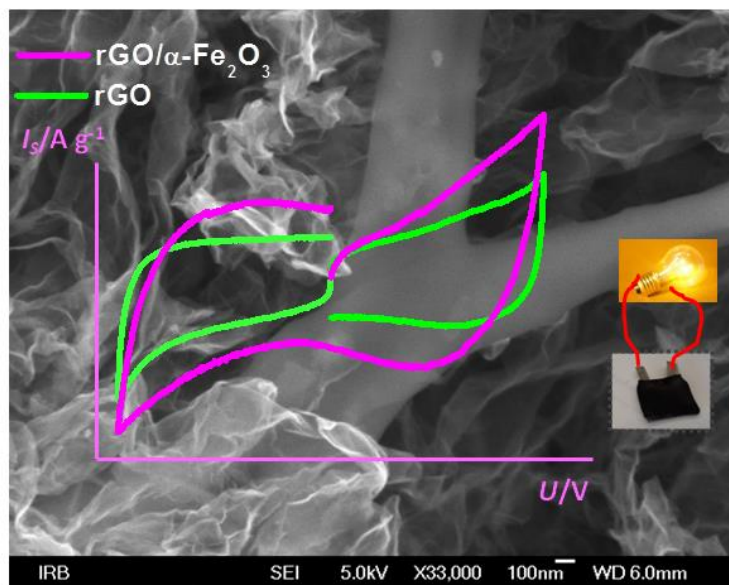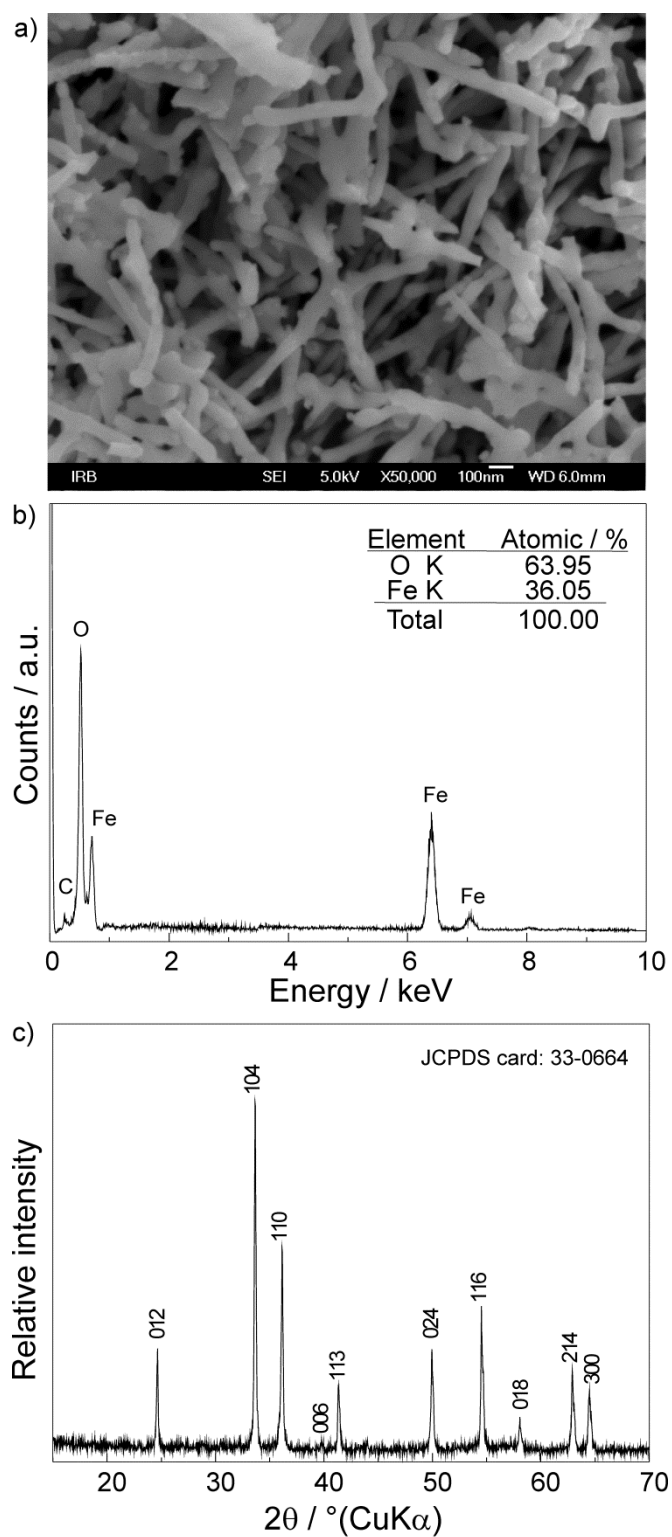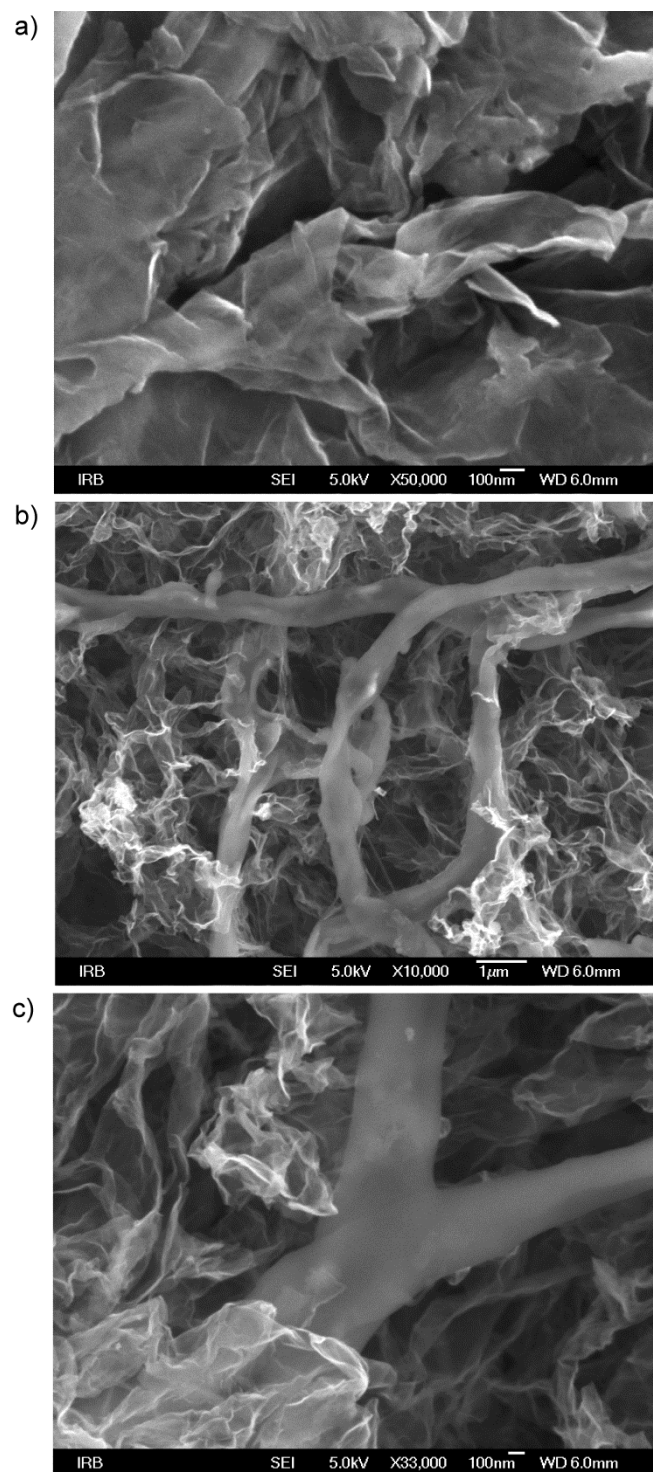
Graphical abstract

Figure 1

a)

b)

Element	Atomic / %
O K	63.95
Fe K	36.05
Total	100.00

c)

JCPDS card: 33-0664

Fig. 1

Figure 2

Fig. 2

Figure 3
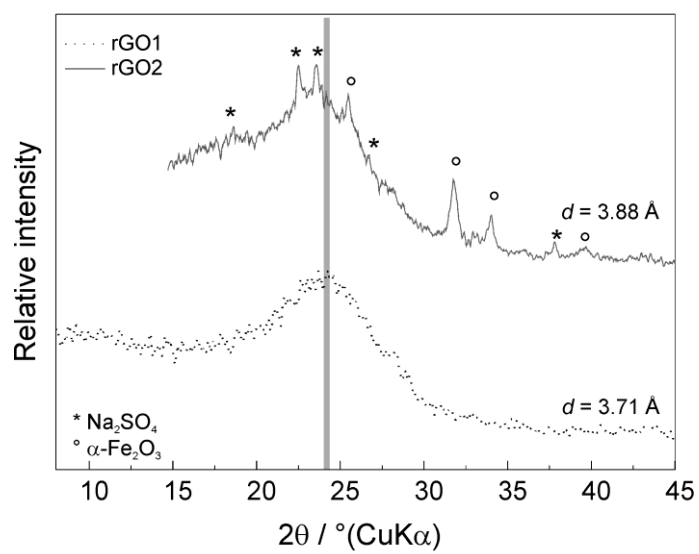
Fig.3

Figure 4
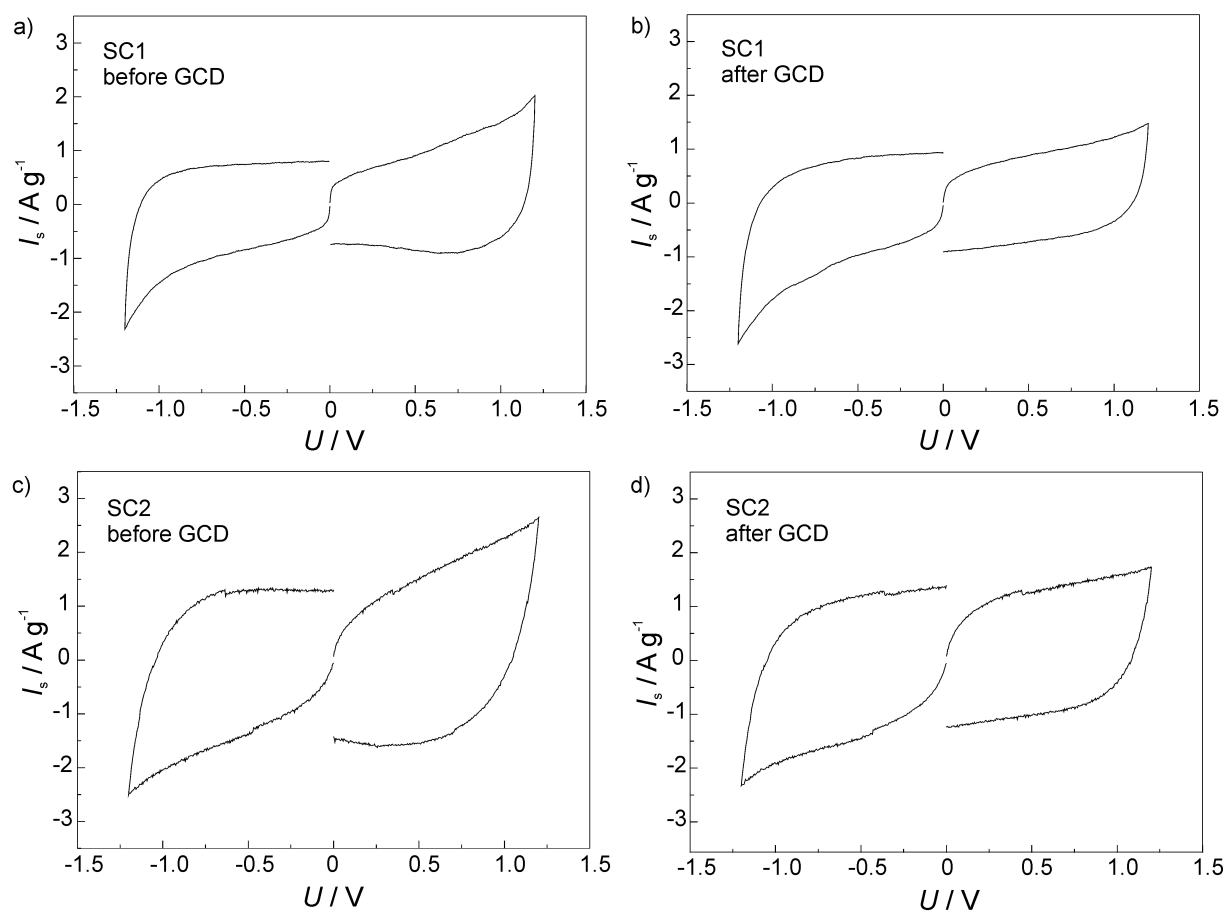
Fig. 4

Figure 5

Fig. 5

Figure 6

Fig. 6